Improved p-type antimony-telluride alloys (Sb_2Te_3) for thermal converters

J. P. Carmo, M. F. Silva, J. F. Ribeiro, L. M. Gonçalves, and J. H. Correia
University of Minho, Department of Industrial Electronics
Campus Azurém, 4800-058 Guimarães, PORTUGAL

ABSTRACT

This focus of this chapter is the presentation of antimony-based materials for thermoelectric applications. Examples of thermoelectric applications are (1) the electrical energy from temperature gradients and (2) cooling devices, but both using solid-state converters. These converters use pairs of thermoelectric p- and n-type materials. In this context, this chapter presents all the fabrication and characterization details of the p-type material. The antimony-based material selected to serve as p-type structures was the Antimony telluride (Sb_2Te_3). The Sb_2Te_3 is a chalcogenide and its thin-film deposition requires a precise controlled process to achieve the highest possible thermoelectric figure-of-merit, *ZT*. This goal is achieved with the co-evaporation of antimony (Sb) and telluride (Te) technique. The optimizations of the Sb_2Te_3 thin-films deposition on a flexible substrate are presented. It is also analyzed the influence of the parameters involved in the depositions (e.g., the temperature which the substrate is subjected, and the evaporation rates of Sb and Te), and their impacts in the final composition of Sb_2Te_3 thin-films.
Some well known techniques of analysis were employed during the measurements for characterizing the quality of Sb_2Te_3 thin-films: X-ray diffraction (XRD), energy-dispersive X-ray spectroscopy (EDX), X-ray photoelectron spectroscopy (XPS) and Raman spectroscopy. The measurements done at the room temperature of 300 K for the best deposited samples showed Sb_2Te_3 thin-films with Seebeck coefficients up to 200 $\mu V.K^{-1}$, an in-plane electrical resistivity in the range [8-15] $\mu\Omega.m$, a carrier concentration in the range $[1\text{-}7]\times10^{19}$ cm^{-3}) and an Hall mobility in the range [120-180] $cm^2.V^{-1}.s^{-1}$.

INTRODUCTION

The thermoelectricity is the conversion of temperature differences in electric energy, and vice-versa. Three effects are included in the thermoelectricity, e.g., the Seebeck, Peltier and Thomson effects. Thomas Seebeck (1770-1831) discovered that a temperature difference between the junction of two different materials makes an electric voltage to arise, and an electric current will start to flow when an electric circuit is closed (Seebeck, 1822). This effect is quantified by the Seebeck coefficient, α [μVK^{-1}]:

$$\alpha = \frac{\Delta V}{\Delta T} \tag{1}$$

Essentially, the Seebeck is used for two type of applications: temperature sensors and thermoelectric (TE) generators (Seebeck, 1822) – see the Figure 1.

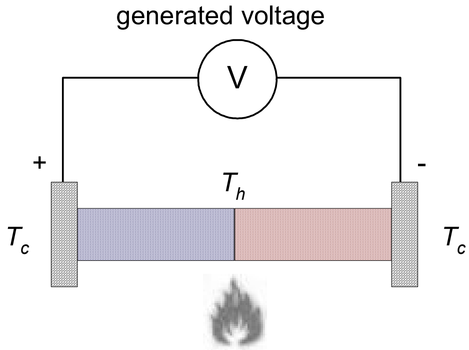

(a) *Temperature sensor*

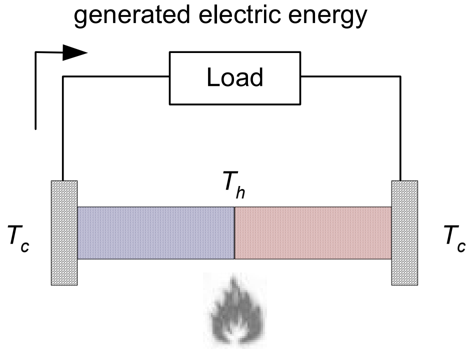

(b) *Thermoelectric generator*

Figure 1: Seebeck effect, used as temperature sensor or energy generator (b).

Jean Peltier (1785-1845) verified in 1834 that the flow of an electric current through the junction connecting two different materials, makes an amount of thermal energy to be released or absorbed by this junction – see the Figure 2 -, and the temperature in this same junction rises or decreases, respectively. Also, he observed that the released or the absorbed energy was proportional to the electric current. This effect is quantified by the Peltier coefficient, π. Some years later, William Thomson (later known as Lord Kelvin) established the relation between the Peltier and Seebeck coefficients:

$$\pi = \alpha . T \tag{2}$$

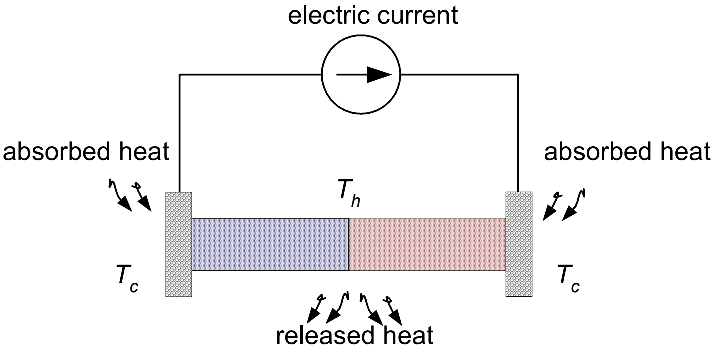

(a) *Heating by Peltier effect*

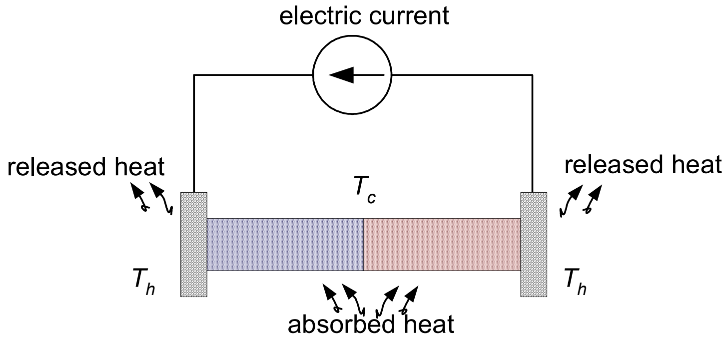

(b) *Cooling by Peltier effect*

Figure 2: Using the Peltier effect for heating or cooling.

MOTIVATION

The thermoelectricity renewed interest with the rise of new materials, both in academic research and in industry. The interest of these areas include cooling applications (for use in laser modules, biomedical applications, chip spot-cooling) and energy generation (in energy harvesting systems) for use in autonomous microsystems, where the use of batteries is not adequate. However and up to now, the research is being essentially focused in the way to get new materials with higher performance (using nanostructures), or to improve the performance of the conventional thermoelectric converters (whose final target is the refrigeration in domestic applications and energy generation in cars by recovering heat lost in the exhaust gases from engine). The integration of these converters with electronic circuits (using the same techniques used to fabricate microsystems) is still in a start-up phase. This chapter presents the fabrication technology of thermoelectric materials made of p-type thin-films of antimony tellurides for use in cooling, infrared radiation detection, and in thermoelectric energy scavenging systems.

MODELLING THERMOELECTRIC MICROSYSTEMS

A planar Peltier microcooler is usually composed of many pairs of PN junctions, like one represented on Figure 3.

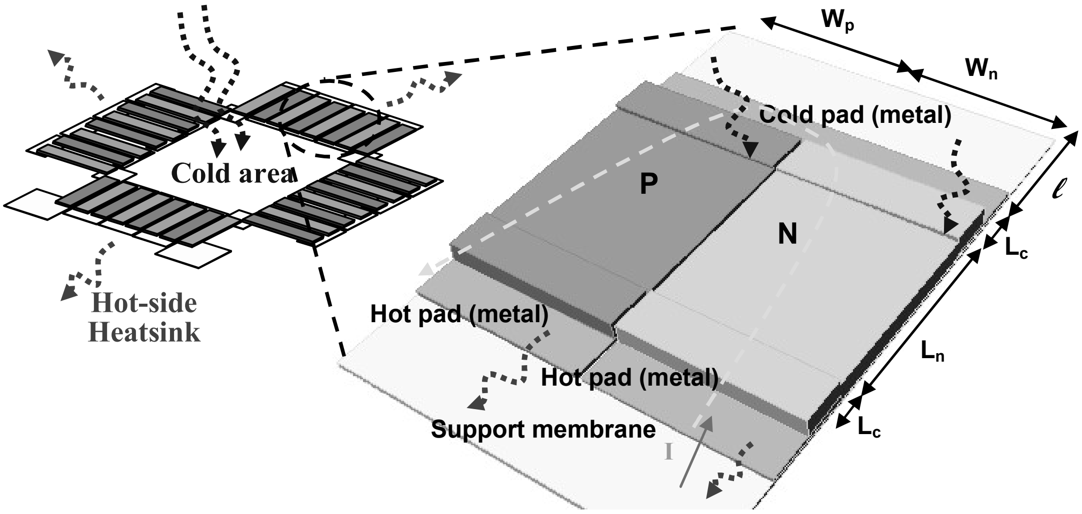

Figure 3: A single cell Peltier planar cooler made of n=16 thermoelectric p-/n-type pairs. Two thermoelectric elements (p- and n-type) connected in series by metal pads stand on top of a support membrane.

The performance of a thermoelectric converter is determined by the figure-of-merit of the materials used (Peltier, 1834):

$$ZT = \frac{\alpha^2 T}{\rho\kappa} \tag{3}$$

where α [VK^{-1}] is the Seebeck coefficient, ρ [Ωm] is the electrical resistivity, κ [Wm^{-1}K^{-1}] is the thermal conductivity and T the temperature. The performance parameter ZT is very useful in Seebeck sensing devices, such as infrared thermal detectors. Another factor is more appropriate for specifying the performance of a TE microconverter, which is the power factor, PF [WK^{-2}m^{-1}]. The PF is defined as the electric power per unit of area through which the heat flows, per unit of temperature gradient between the hot and the cold sides, and is expressed as:

$$PF = \frac{\alpha^2}{\rho} \tag{4}$$

The device illustrated in the Figure 3 is a planar thermoelectric converter that was fabricated on top of a kapton foil with a thickness of 25 μm. The maximum power provided by a thermoelectric device with n thermoelectric pairs when subjected to a thermal gradient ΔT [K] is given by:

$$P_{MAX} = \frac{[n^2(\alpha_p - \alpha_n)^2 - \Delta T]^2}{4nR} \tag{5}$$

The Figure 4 shows the maximum power and the maximum voltage that can be provided by a four pair thermoelectric device made of p- and n-type materials with figures-of-merit, ZT, at room temperatures of 0.5 and 0.84, and power factors of 2.81×10^{-3} WK^{-1}m^{-2} and 4.87×10^{-3} WK^{-1}m^{-2}, respectively. The p-type materials are made of antimony tellurides and are the focus of this chapter.

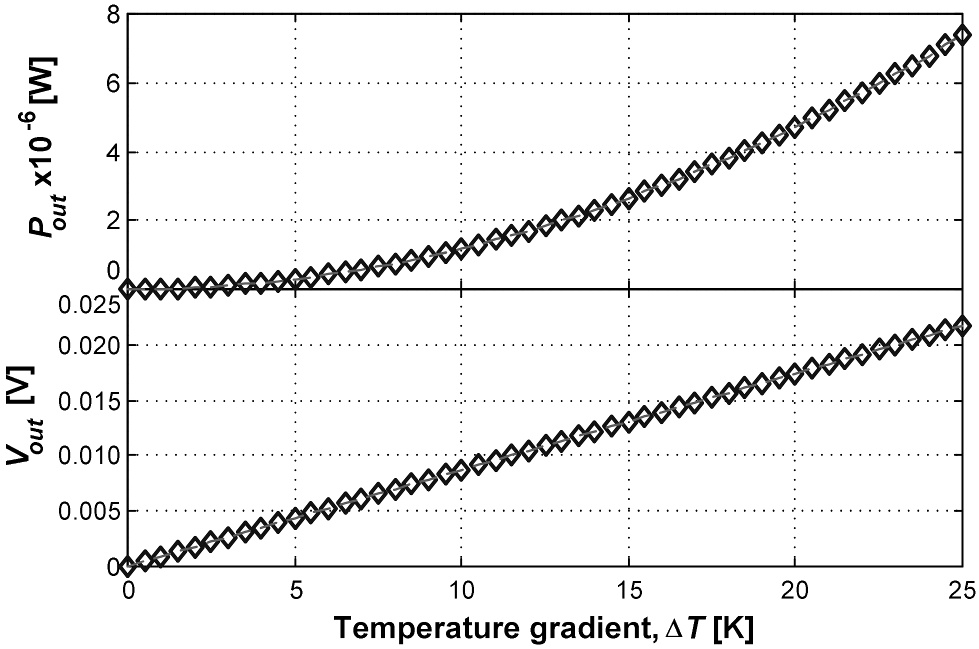

Figure 4: For a thermoelectric converter with four pairs: the maximum power and the maximum voltage at its output terminals.

ANTIMONY TELLURIDE DEPOSITIONS

This section focuses on the deposition and characterization of p-type Sb_2Te_3 thin films. It was demonstrated before that the direct evaporation of the bulk materials results in a compositional gradient along the film thickness due to the large differences in vapour pressure of antimony (Sb) and tellurium (Te) (da Silva *et al* 2002, da Silva *et al* 2005). Other deposition processes have been reported in the literature for the deposition of Sb_2Te_3 thin films. Co-sputtering, electrochemical deposition, metal-organic chemical vapour deposition or flash evaporation are some examples. Zou *et al* (Zou *et al*, 2002) fabricated p-type Sb_2Te_3 films, and reported the influence of substrate temperature and evaporation rate of the materials during the film growth, on the electronic properties. In the present work, the influence of growing parameters (evaporation rates of Sb and Te and substrate temperature) is studied in detail. Glass, silicon and polyimide were used as substrates, with good film-to-substrate adhesion. However, for thermoelectric applications, 25 µm-thick Kapton film was chosen as substrate because of the low thermal conductivity (as low as 0.12 $W.m^{-1}.K^{-1}$) and appropriate value of thermal expansion coefficient (12×10^{-6} K^{-1}) which closely matches the thermal expansion coefficient of the telluride films, thus reducing residual stress and increasing adhesion.

Experimental

The antimony telluride thin-films were deposited by co-evaporation using resistive heating in a high-vacuum chamber - see the Figure 5(a). The power applied to each evaporation boat (made of molybdenum) was controlled independently by way of two Proportional Integral Derivative (PID) (Zou *et al*, 2002) controllers to maintain a constant deposition rate at a certain setting during deposition. The Sb/Bi evaporation flow rate, Fr_{Sb}/Fr_{Bi} [$nm.s^{-1}$], and Te evaporation flow rate, Fr_{Te} [$nm.s^{-1}$], allow tuning of the ratio of the evaporation flow-rates, R, which is given by: $R=Fr_{Te}/Fr_{Sb}$ or $R=Fr_{Te}/Fr_{Bi}$, which is basically the amount of Te divided by the amount of Sb that is actually being deposited at the substrate surface during co-evaporation.

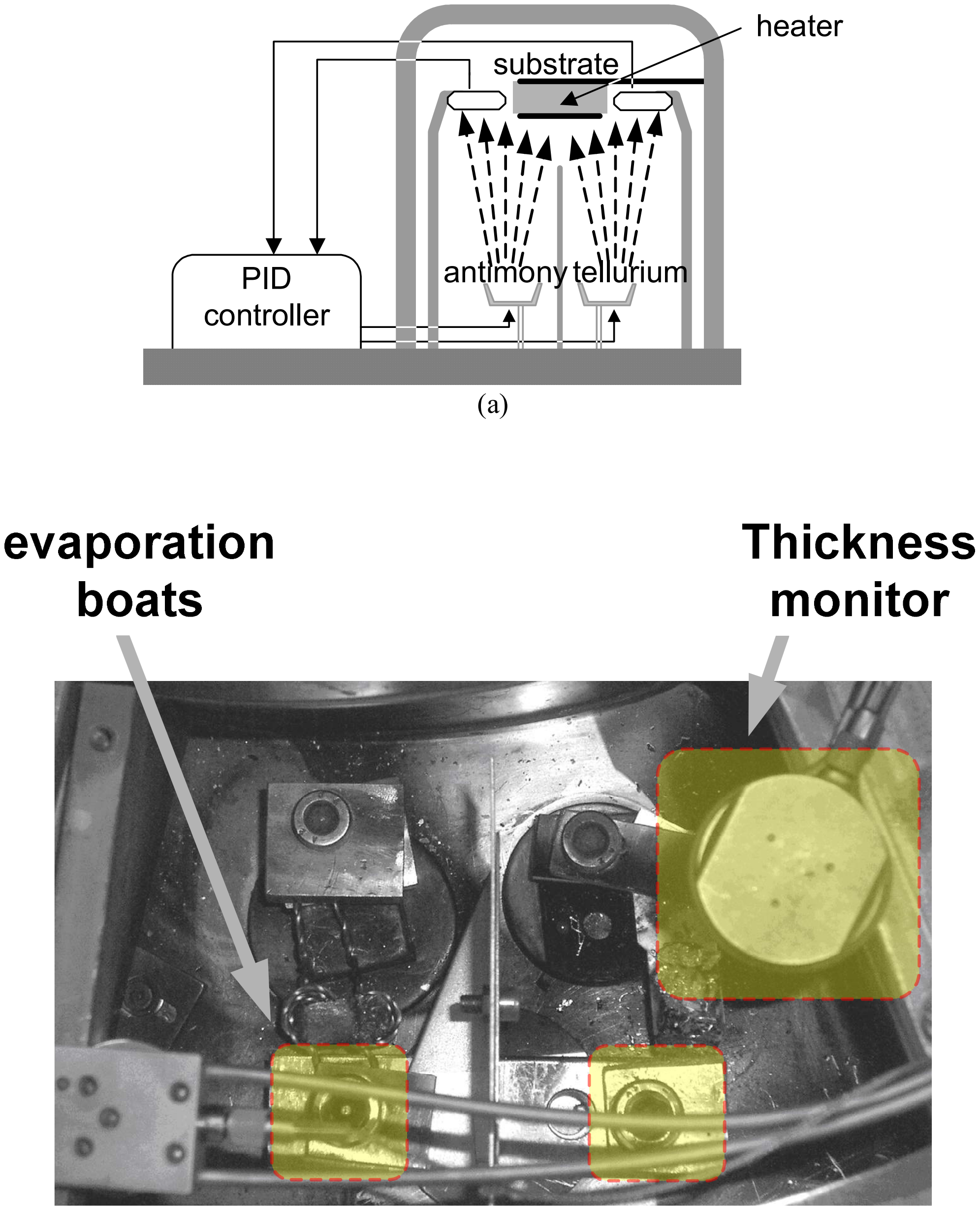

(a)

(b)

Figure 5: (a) The co-evaporation system; (b) the boats and the mass sensors placed inside the co-deposition chamber. These figures were reproduced with previous authorization of the publisher (Elsevier Science Direct).

Each PID controller reads the deposition rate from a thickness monitor (acting as a mass sensor) and was designed to compute the power necessary to be applied to the corresponding evaporation boat in real time in order to maintain the desired evaporation rate. The signals at the output of each mass sensor (see the

Figure 6 that shows the schematic of this read-out circuit) are periodic with an oscillation frequency, f [Hz]. The amount of material accumulated in the surface of each mass sensor is proportional to the thickness, h [m], of deposited Te (or Sb). Such a relation is given by $h=(N_Q d_Q)/(\pi d_F Z f)\times\mathrm{arctg}[Z.\tan(\pi(f_Q-f)/f_Q)]$, with $Z=[(d_Q S_Q)/(d_F S_F)]^{1/2}$, where N_Q=1668 Hz.m is the frequency constant of a crystal made of quartz, d_Q=2688 Kg.m^{-3} is the density of the quartz material, d_F [Kg.m^{-3}] is the density of deposited material (Te or Sb), Z is a material constant, f_Q [Hz] is the output frequency before the deposition, S_Q=300 Kg.m^{-1}s^{-2} is the shear modulus of the quartz material, and S_F is the shear modulus of deposited material. The values of d_F and Z-factor for Te and Sb are: 6250 Kg.m^{-3} at Z=0.90 and 6620 Kg.m^{-3} at Z=0.77. A metal sheet was placed between the two boats to partially separate the flows from the two evaporated species to prevent mixing of the materials at the quartz crystals - see the Figure 5(b). Large boats (baffled boxes with a volume of 4 cm^3) were used to keep the evaporation rates stable. The substrates were heated to temperature setpoints, T_{sub} [ºC], between 150 ºC and 220 ºC.

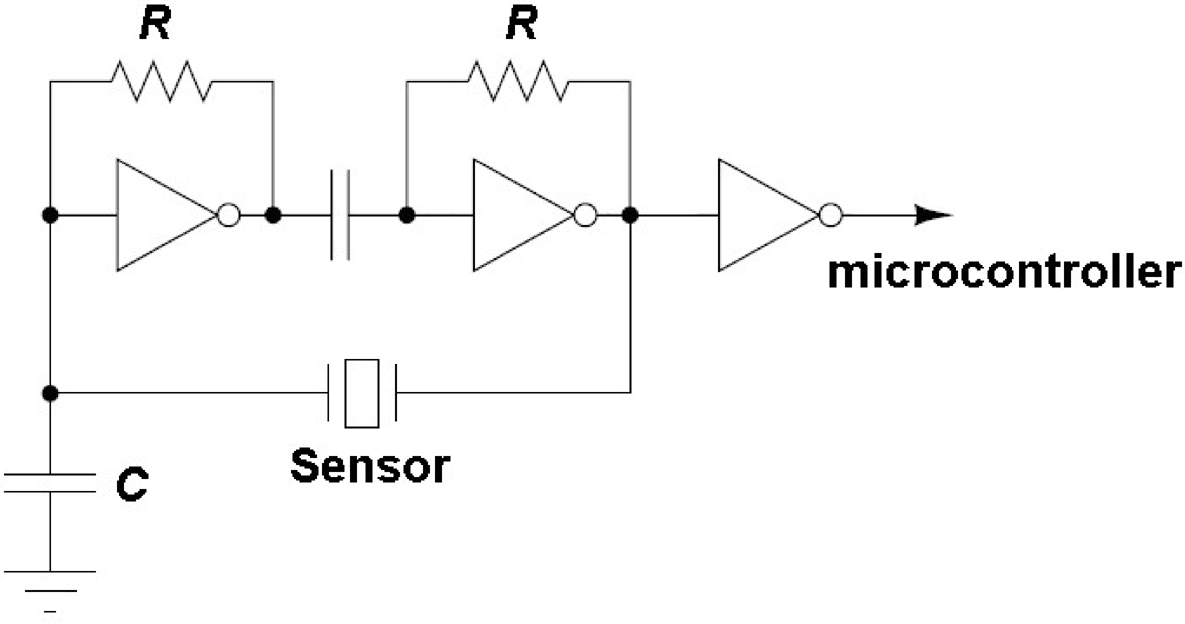

Figure 6: The schematic of the readout circuit of the mass sensors

Each evaporation boat is heated by an AC electrical signal with voltage in the range 2-6 V and current in the range 50-60 A, respectively. The PID controllers were implemented, using the P89C51RD2 microcontroller from Philips Semiconductors. Basically, the PID controllers adjust the power by switching of two independent sine waves at a particular phase angle. The photograph of the control circuit (e.g., the two PID controllers) is in the Figure 7(a). The Figure 7(b) shows the schematic of the electronic circuit responsible to do the phase detection of the power line voltage. The electronic circuit illustrated in the Figure 7(c) is the schematic of the triac switching circuit, whose switching angle is controlled by the microcontroller with the help of an optocoupler. This circuit is responsible for controlling the voltage applied to the primary winding of a power transformer. The secondary winding of the transformer is directly connected to the evaporation boat. Finally, the Figure 7(d) shows the controlled 50 Hz voltage supplied to one of the evaporation boats.

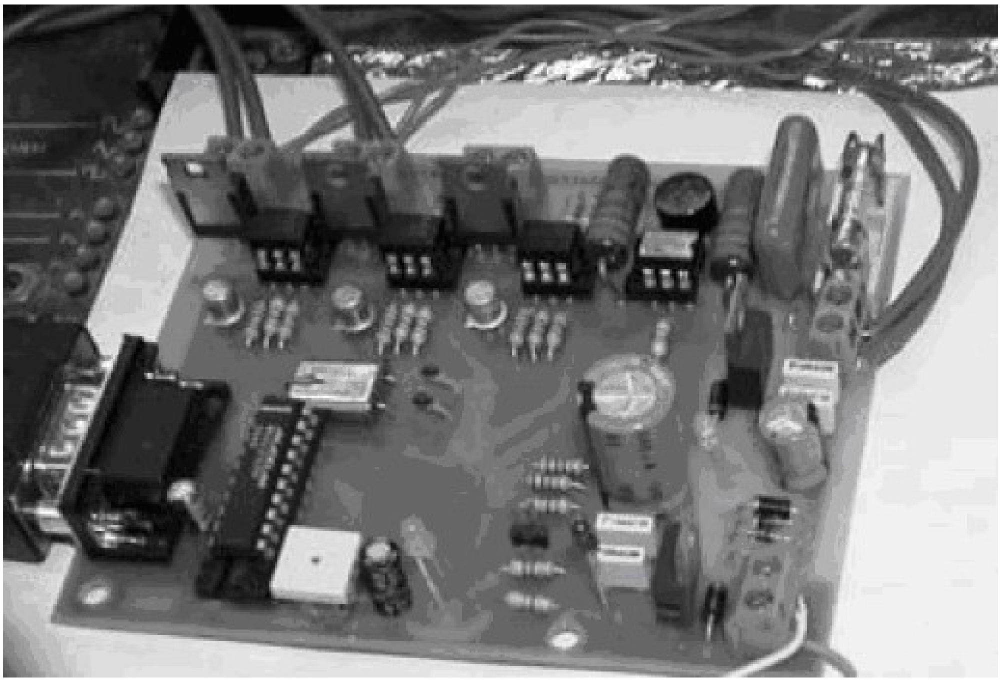

(a)

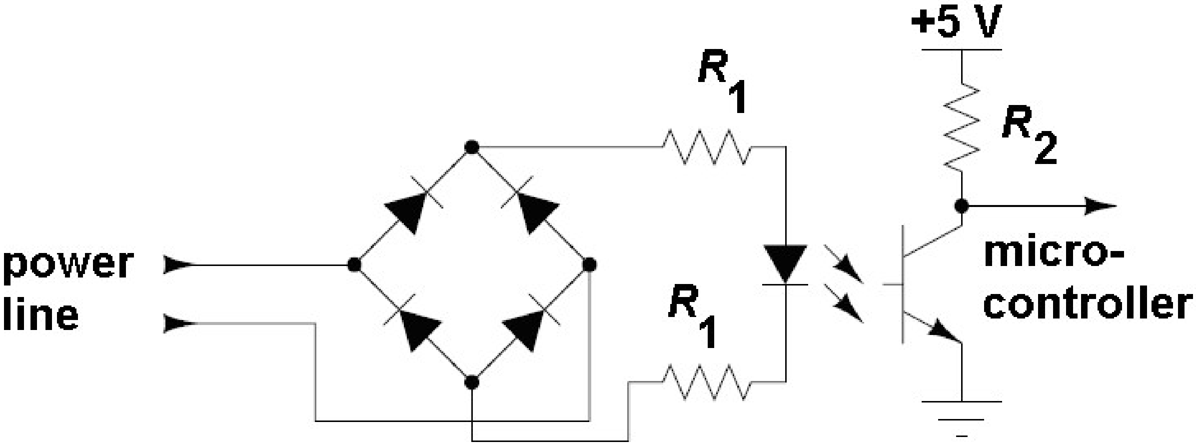

(b)

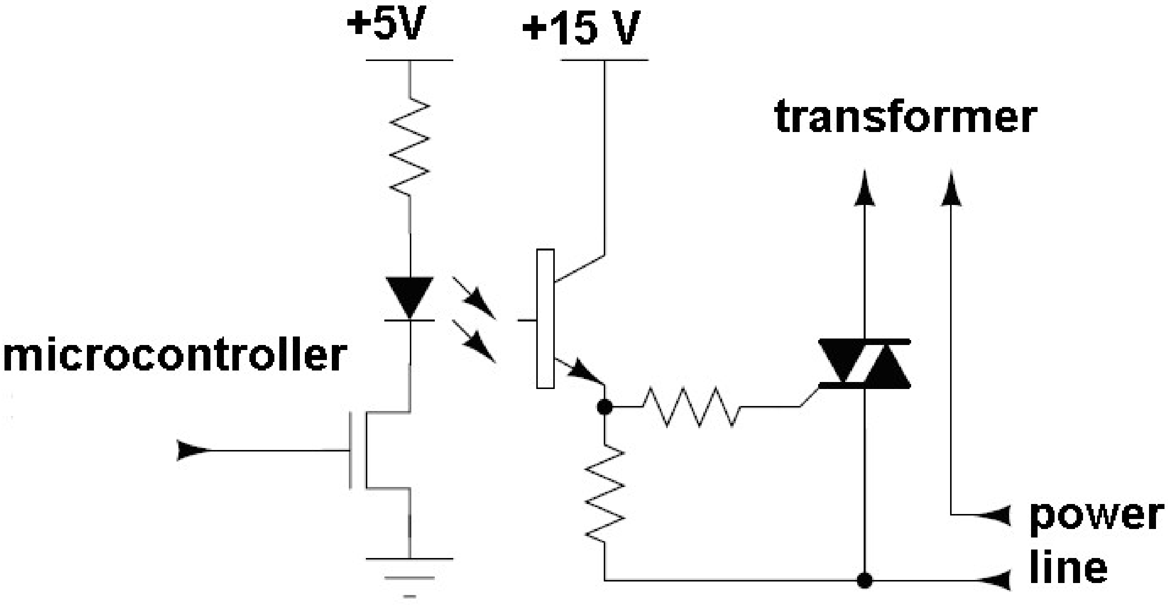

(c)

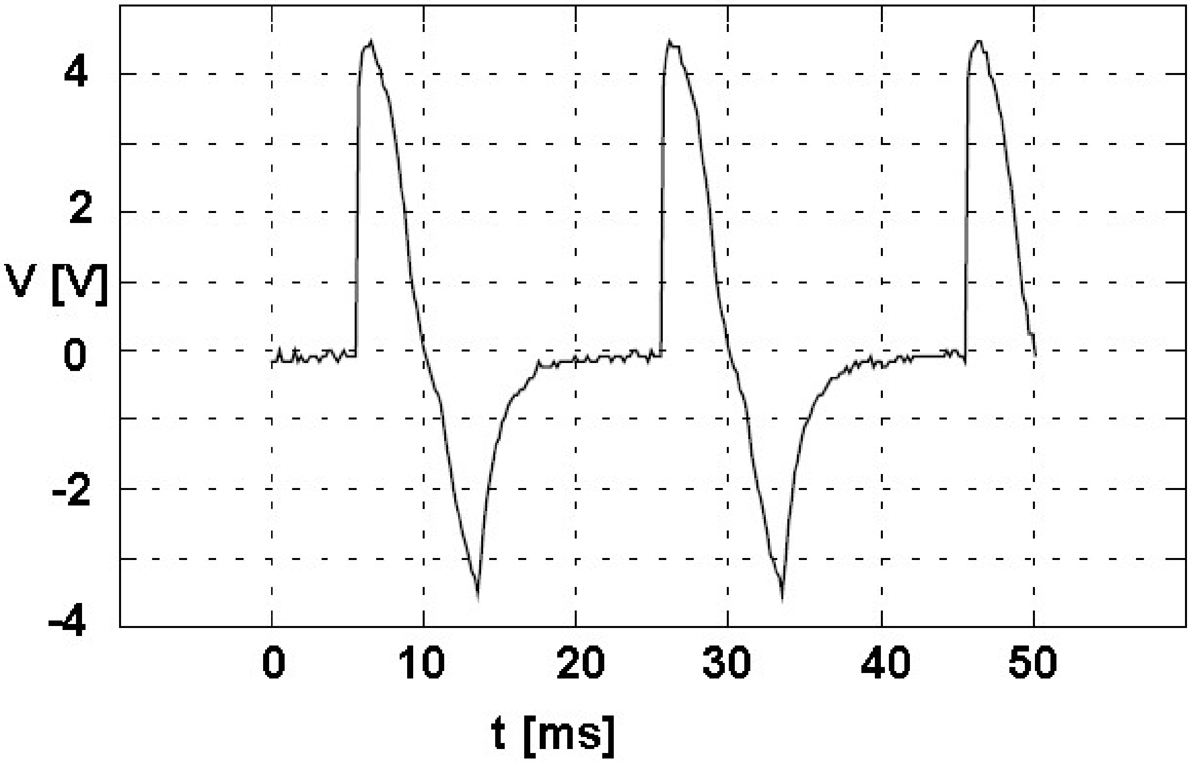

(d)

Figure 7: (a) A photography showing the control circuit. (b) The schematic of the circuit responsible for doing the phase detection of the power line voltage. (c) The schematic of the power switching circuit. (d) The voltage acquired from one of the evaporation boats, for a conduction angle of 100º.

Results

Several films of Sb_2Te_3 were deposited with different flow rate ratios, R, and substrate temperatures, T_{sub}, in order to study the effect of these parameters on the thermoelectric properties of the films. R was set by fixing the Sb evaporation flow rate, Fr_{Sb}, at 2 Ås^{-1} and varying the Te evaporation flow rate, Fr_{Te}, in the range 3-9 Ås^{-1}. Three series of films were fabricated, at T_{sub}=150, 180 and 220 ºC. All films were approximately 1 μm thick (accepting a tolerance of ±30%). The Table I summarizes the thermoelectric properties of selected Sb_2Te_3 films.

Table I: Properties of selected Sb_2Te_3 films. This table was reproduced with previous authorization of the publisher (Elsevier Science Direct).

Film	T_{sub} **[ºC]**	$R=F_{Te}/F_{Sb}$	**%Te by EDX**	α **[μVK^{-1}]**	ρ **[μΩm]**	n **[10^{19} cm^{-3}]**	μ **[cm^2 V^{-}1 s^{-1}]**	$PF\times10^{-3}$ **[WK^{-2}m^{-1}]**
#195C	150	1.47	54.5%	91	7.6	12.5	65.5	1.09
#305A	150	1.67	61.4%	140	14.0	2.4	185.8	1.40
#305D	150	2.13	64.7%	191	31.2	2.0	174.3	1.17
#197D	150	2.35	64.4%	137	43.6	4.6	31.1	0.43
#198A	180	1.85	60.4%	134	24.4	9.0	28.4	0.74
#198B	180	2.02	59.1%	158	30.3	1.44	143.2	0.82
#198D	180	2.35	62.4%	156	39.1	2.0	78.8	0.62
#304A	220	1.67	64.1%	81	10.5	25.3	23.5	0.63
#304D	220	2.13	61.2%	133	10.0	3.6	174.3	1.78
#306A	220	2.50	67.3%	156	9.2	4.1	166.4	2.66
#306D	220	3.18	73.5%	188	12.6	4.3	115.2	2.81

X-ray diffraction (XRD) reveals the polycrystalline structure of Sb_2Te_3, as shown in the Figure 8. The peaks agree with the powder diffraction spectra (JCPDS, 1983) for polycrystalline Sb_2Te_3 (15-874) and similar results from XRD analysis can also be found in literature (da Silva, 2005). The difference on X-ray diffraction patterns on the two films analyzed could be due to differences on composition and substrate temperature. Film #305 was deposited at T_{sub}=150 ºC and films #304 and #306 were deposited at T_{sub}=220 ºC. The tellurium content in the composition was 63% of films #304 and #305 and 70% on film #306.

The planes with higher intensity obtained in films deposited at T_{sub}=220 ºC (#304 and #306) are not the same from films deposited at T_{sub}=150 ºC (#305) or from bulk Sb_2Te_3. The substrate temperature during deposition influences the structure and orientation of Sb_2Te_3 thin-films. Tellurium phase is also detected in films with higher Te content (#306). The SEM cross-sectional and surface images of the material also reveal the polycrystalline structure of the films and the effect of substrate temperature on polycrystalline morphology (see the Figure 9).

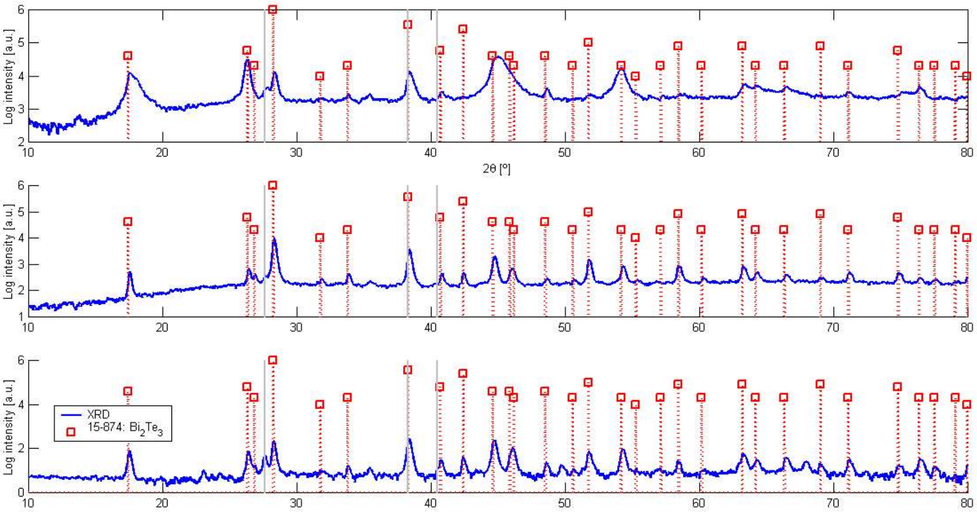

Figure 8: XRD planes of powdered crystalline bulk Sb_2Te_3 detected on films #304, #305 and #306. The gray-shaded vertical lines represent the positions of tellurium (Te) diffractograms on the XRD.

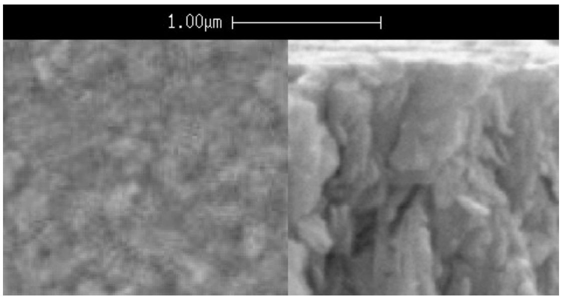

Figure 9: Surface and cross-sectional SEM images of $Sb2_2Te_3$ thin-films deposited on glass.

The XPS analysis was performed at on a Sb_2Te_3 thin-film with 1 μm thickness (Gonçalves *et al*, 2011). Ion etching during analysis was performed at low energy, to avoid heating the films and lose original composition, due to different vapour pressures of Sb and Te. Composition was measured as function of film deep and results present the contamination (carbon) and oxidation of film surface, up to 50 nm deep. Composition measured deeper thickness corresponds to that obtained by EDX. Composition measurements were also confirmed by RBS/PIXIE technique.

The film composition is always poorer in Te than the corresponding fraction of evaporated Te, *R*. This effect is more noticeable as T_{sub} increases. At 220 ºC, the vapour pressure of Te is $10^3\times$ higher than the vapour pressure of Sb. Therefore, it is possible to conclude that re-evaporation of Te from the substrate proceeds at a higher rate than Sb. This explains why it is necessary to use a higher value of *R* than the desired atomic ratio of Te/Sb in the final film composition. Since the Te percentage on the films is always small than the corresponding percentage of evaporated Te and it also depends on substrate temperature, it's difficult to obtain the desired stoichiometry. The evaporation rate of tellurium must be adjusted to overcome these factors, in order to obtain the desired final stoichiometry.

The Figure 10(a) shows the dependence of the Seebeck coefficient on the flow rate ratio (*R*), for films deposited at different substrate temperatures (150 ºC, 180 ºC and 220 ºC). It was not noted relevant dependence of the substrate temperature (T_{sub}) on the value of Seebeck coefficient but the value of this coefficient increases as R is increased.

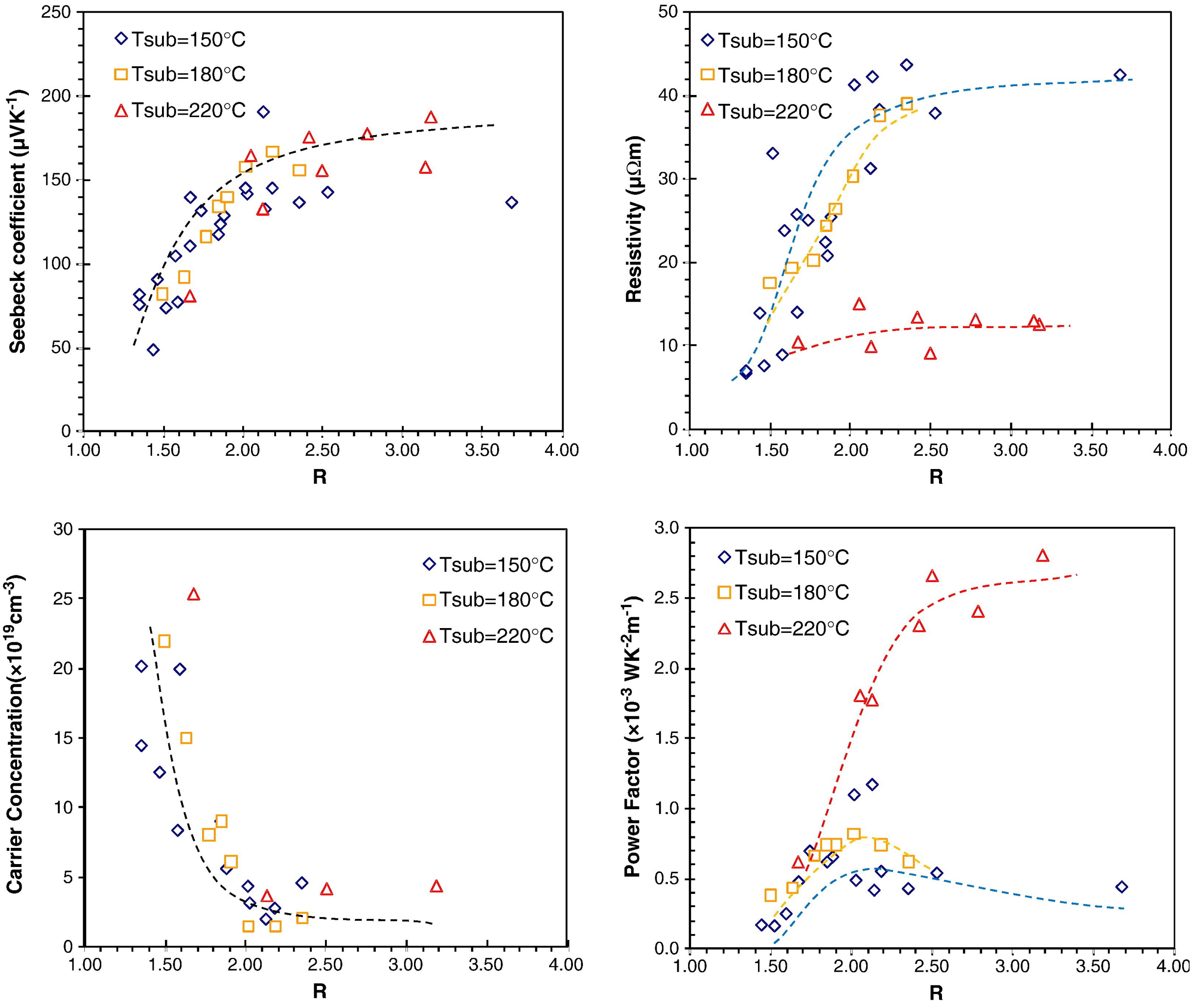

Figure 10: (a) The Seebeck coefficient of Sb_2Te_3 thin films as a function of Te/Sb evaporation flow ratio, R. (b) The electrical resistivity of Sb_2Te_3 as a function of Te/Sb evaporation flow rate ratio, R. (c) The carrier concentration and Hall mobility of Sb_2Te_3 as a function of Te/Sb evaporation flow rate ratio, R. (d) The power factor of Sb_2Te_3 as a function of Te/Sb evaporation flow rate ratio, R. (Gonçalves et al, 2011). This figure was reproduced with previous authorization of the publisher (Elsevier Science Direct).

The Figures 10(b) and 10(c) show the electrical resistivity, the carrier concentration and the Hall mobility of Sb_2Te_3 films as a function of R for different T_{sub}. There is a strong dependence of electrical resistivity with T_{sub}. Lower electrical resistivity is obtained with substrate temperature above 220 ºC. In order to achieve high power factors, *PF*, a low carrier concentration with high mobility is desirable. Films with composition rich in tellurium have lower carrier concentration (less than 5×10^{19} cm^{-3}) and higher Seebeck coefficients. High mobility (higher than 100 cm^{2}V^{-1}s^{-1}) is obtained with R between 2 and 3. At each T_{sub} the maximum value of power factor is also obtained at a value of R that depends on T_{sub} - see the Figure 10(d).

The maximum *PF* is obtained at R=2 for T_{sub}=150 ºC or T_{sub}=180 ºC. For T_{sub}=220 ºC, the maximum *PF* is obtained with R=3. On thin films, resistivity and Seebeck coefficient are higher than on bulk crystal, respectively $\rho_{11}\approx 1.9\,\mu\Omega$m α_{11}=83 µVK^{-1} (Scherrer *et al*, 2005). On the other way, carrier concentration and Hall mobility was lower than those values on bulk Sb_2Te_3, respectively n=10.6×10^{19} cm^{-3} and μ=313 cm^{2}V^{-1}s^{-1} (Scherrer *et al*, 2005). The influence of substrate temperature on power factor was also analysed (Gonçalves *et al*, 2011) and comparable results obtained by da Silva (da Silva *et al*, 2005) and Zou (Zou *et al*, 2002) on the same materials are also presented. The highest value of PF=2.8×10^{-3} WK^{-2}m^{-1} was obtained in films deposited at T_{sub}=220 ºC with Sb evaporation rate of 2 Ås^{-1} and Te evaporation rate of 6.4 Ås^{-1} (R=3.2). These evaporation parameters resulted in tellurium rich composition (measured by EDX) of the compound with 25-35% of Sb and 65-75% of Te. The power factor versus the composition, measured by EDX, for different substrate temperature was also analysed (Gonçalves *et al*, 2011). The power factor of Sb_2Te_3 bulk crystal and thermal evaporated thin-film obtained by other authors (da Silva *et al*, 2005) are also plotted. The value of *PF* measured on films deposited by co-evaporation at low substrate temperature is lower than this obtained in bulk materials. But with T_{sub}=220 ºC, this value is near those obtained in bulk Sb_2Te_3. Higher *PF* value was measured with tellurium rich films (70% Te on composition).

The thermal conductivity, κ, was measured in one Sb_2Te_3 film, using the method described by Völklein (Völklein *et al*, 1997). The value of 1.8 Wm^{-1}K^{-1} was obtained. Thermal conductivity is due to electron and phonon contribution effects, respectively κ_e and κ_p ($\kappa=\kappa_{e+}\kappa_p$). Electron contribution could be estimated through Wiedemann-Franz law, $k_e=LT/\rho_e$, where L is the Lorenz number, T the temperature and ρ_e is the electrical resistivity. Considering L=2.1×10^{-8} V^{2}K^{-2} (Dyck *et al*, 2002) and ρ_e=15 µΩm, at 300 K, κ_e=0.42 Wm^{-1}K^{-1} and κ_p=1.38 Wm^{-1}K^{-1}. These values are comparable to those on bulk Sb_2Te_3 ($\kappa\approx$4 Wm^{-1}K^{-1}, parallel to crystal planes and e $\kappa\approx$1 Wm^{-1}K^{-1}, perpendicular to crystal planes). With the measured value of Seebeck coefficient on this film (α=160 µVK^{-1}) the figure-of-merit value ZT=0.3 was obtained.

Discussion

P-type Sb_2Te_3 thermoelectric thin films with high figure-of-merit were fabricated by thermal co-evaporation. The best films have a Seebeck coefficient of 188 µV.K^{-1} and a resistivity of 12.6 µΩm of which represents a power factor of 2.8×10^{-3} WK^{-2}m^{-1}. The films were deposited onto glass substrates and flexible Kapton substrates, with good adhesion. The influence of evaporation rates and substrate temperature on composition, Seebeck coefficient, electrical resistivity, Hall mobility and carrier concentration was reported. EDX results show that films with high power factor are obtained when the composition of film is tellurium rich (30% Sb, 70% Te for Sb_xTe_{1-x}). The highest thermoelectric power factor for Sb_2Te_3 thin films was obtained at substrate temperature around 220ºC, Sb evaporation rate of 2 Ås^{-1} and Te evaporation rate of 6.4 Ås^{-1}. A thermal conductivity of 1.8 Wm^{-1}K^{-1} as measured and a figure-of-merit at room temperature of ZT=0.3 calculated. These results are comparable with the best published results for the same material (Goncalves *et al*, 2008a).

DEVICES AND APPLICATIONS

The Figure 11 shows a thermoelectric device made with four pairs of p-type (Sb_2Te_3) and n-type (Bi_2Te_3) materials, whose maximal power and voltage behaviors under optimal conditions were presented in the Figure 3. Two applications can be implemented with these thermoelectric converters. The first one is an on-chip array of thermoelectric Peltier microcoolers array (Goncalves *et al*, 2008b). The second application consists on a thermoelectric energy scavenging microsystem to convert the small thermal power available in human-body. A thin-film battery is integrated in the same device as well as ultra low-power electronics to charge the battery and to perform DC-DC conversion (Carmo *et al*, 2009).

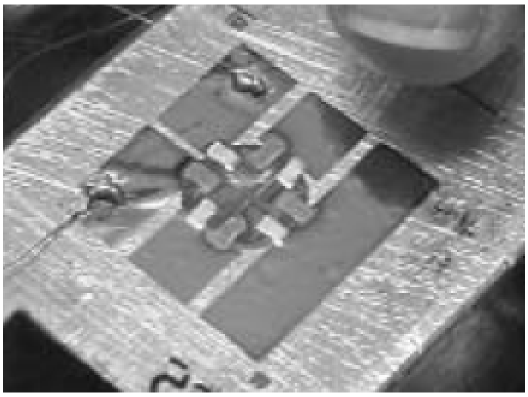

Figure 11: A photograph showing a thermoelectric converter made with four pairs of planar thermoelectric p- and n-type materials. The p-type materials are the Sb2Te3 thin-films presented in this chapter.

On-chip array of thermoelectric Peltier microcoolers

As show in the Figure 12, the array of microcoolers can accommodate up to 64 pixels organised in a 8×8 structure (Goncalves *et al*, 2008a). Each pixel can be independently controlled to heat or cool. The Figure 13 illustrates a single pixel cross-section. When a current flows from the n-type thermoelectric element (TE) to the metal cold pad and from this to the p-type TE, by Peltier effect, heat is absorbed in the metal-TE element junctions. The reverse applies to contact pads on electronics, where heating is generated by Peltier effect.

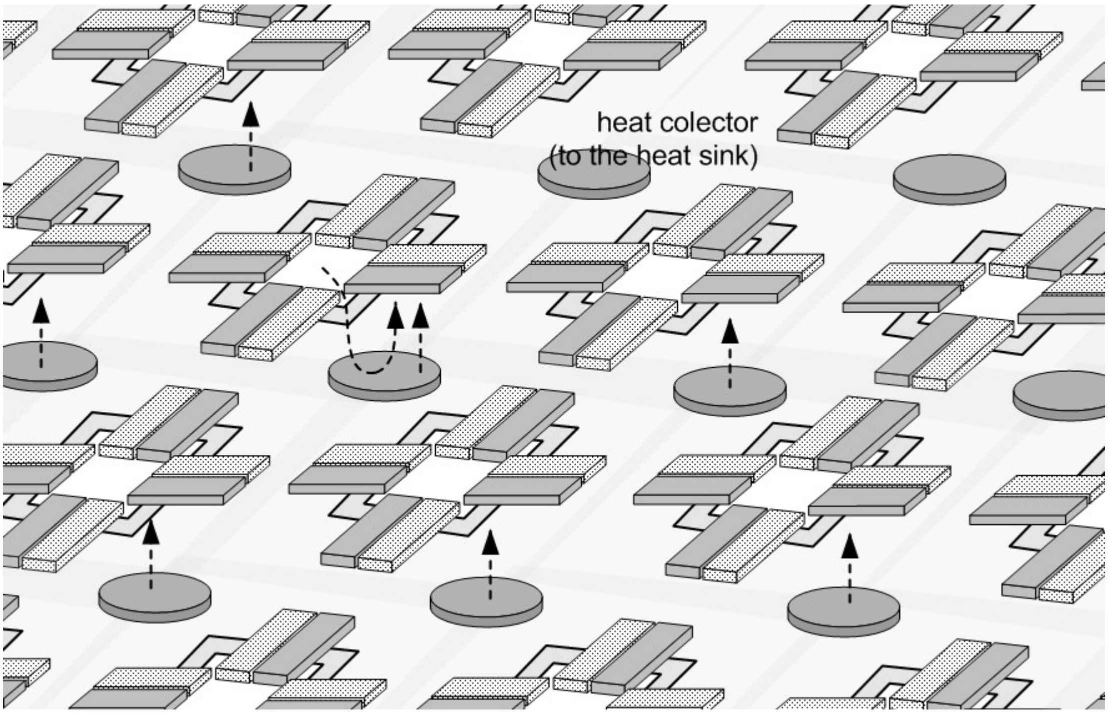

Figure 12: An artist impression showing a part of the microcoolers array. In this artwork, the heat is collected by each pixel (constituted by 4 thermoelectric n-/p-type material pairs) on bottom of the

supporting membrane and directed to the heat collectors (on top of the supporting membrane), to be dissipated in a heat sink (the heat flow from the bottom to the top is represented with dashed lines and arrows).

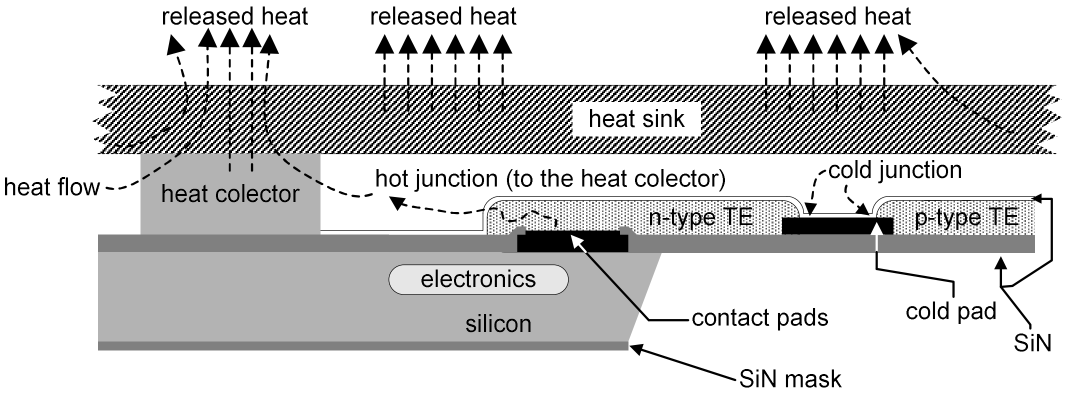

Figure 13: Drawing of a pixel of the microcooler array (it isn't on scale).

A Finite Element Method (FEM) simulation was used to calculate the expected temperature drop on each pixel. A temperature drop of 15 ºC, bellow room temperature was obtained (see the Figure 14). To obtain this cooling capacity, a membrane (200-nm thick) of silicon nitride supports four pairs of thermoelectric elements (40 µm×100 µm×10 µm), powered with 14 mA current. Contact resistivity (between thermoelectric elements and metal pads) of 10^{-10} Ωm^{-2} was assumed on simulations (da Silva *et al* 2004, Birkholz *et al* 1987). Radiation and convection was considered on the cooled surface (10 $Wm^{-2}K^{-1}$). Thermoelectric properties of n-type and p-type elements were considered as achieved on previous experimental results (Goncalves *et al* 2006a, Goncalves *et al* 2006b). The results obtained from the FEM simulation on a single pixel microcooler agree with the theoretical calculations.

A CMOS microchip was designed, with the electronics to address and control each pixel of the array, memorising the state of microcooler. However, the explanation of these electronic circuits is outside of the scope of this chapter.

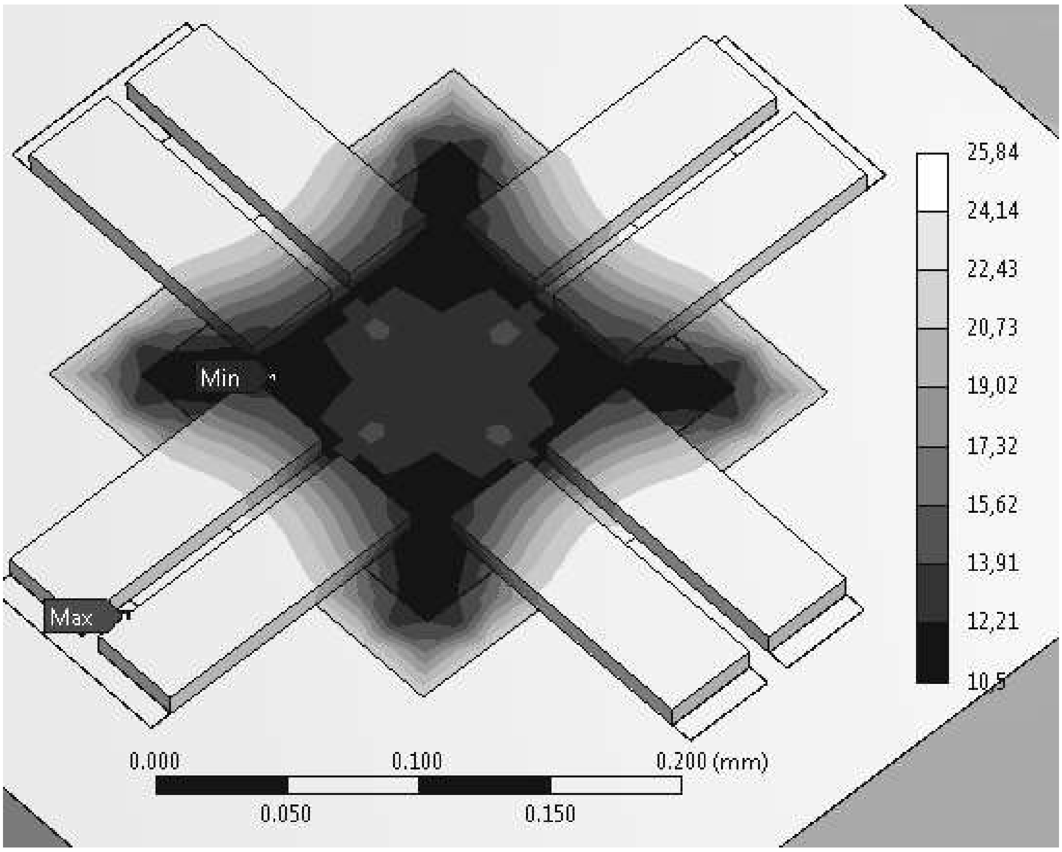

Figure 14: A single pixel microcooler simulation obtained by FEM that shows the possibility to obtain 15 ºC of cooling at the centre of the pixel.

THERMOELECTRIC CONVERTERS WITH SOLID-STATE BATTERIES

The present-day battery technologies are being outpaced by the ever-increasing power demands from new applications, as well as being inherently safe, batteries of the future will have to integrate the concept of environmental sustainability (Armand *et al*, 2008), thus thin-film solid-state batteries are ideal candidates for such purposes. This type of battery shows a very high life cycle and is intrinsically safe. Also, this is of special concern in the design of thermoelectric energy scavenging microsystem, especially when the thought applications are in the biomedical field, or for long cycle operations without requiring human activity. This meets the target related of the proposed thin-film rechargeable battery, which is to use it together with a single-chip regulated thermoelectric power source, which must operate from low temperature gradients (a minimum temperature difference of 3 ºC between ambient and target thermo-source must provide an IC-compatible voltage). In fact, the target objective is to have thermoelectric sources to provide power densities of 10-50 μWcm^{-2}, with temperature gradients of 3-10 ºC.

The Figure 15 shows an artwork of a thermoelectric microconverter with a solid-state battery placed on the top. Practical thermoelectric generators connect large number of junctions in series to increase the operating voltage.

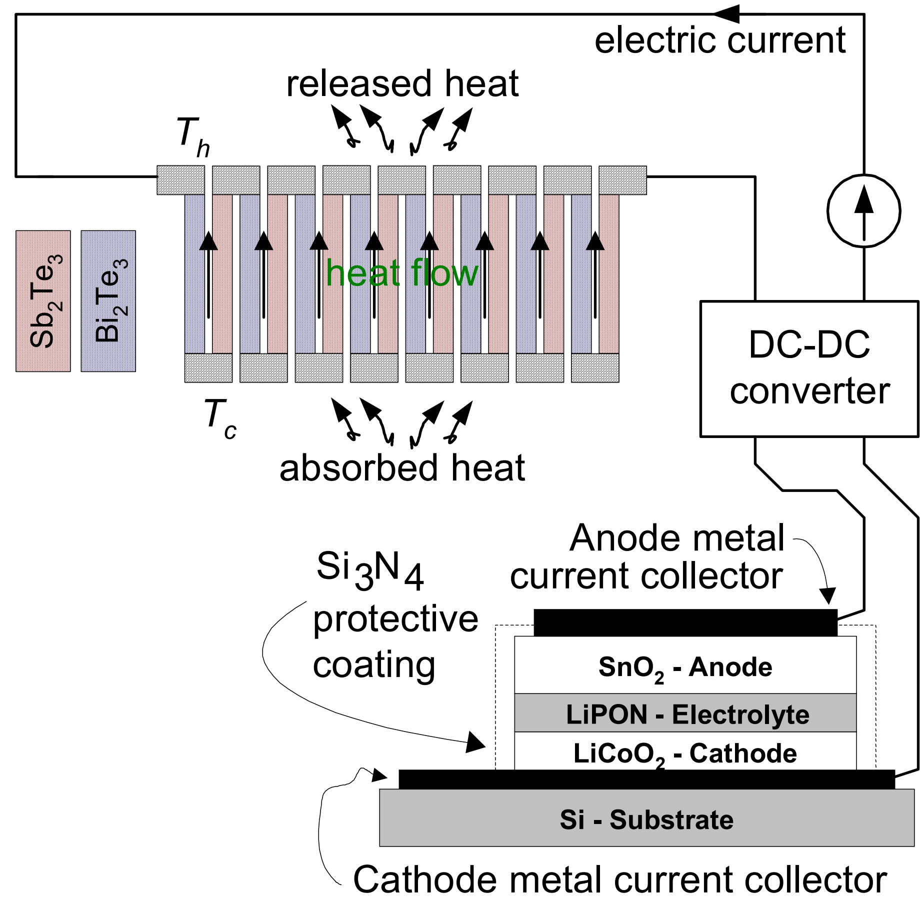

Figure 15: An artist impression showing the integrated power concept, composed by a thermoelectric converter, electronics of power conversion and a solid-state thin-films battery.

A reactive sputtering technique was used in the thin-films depositions. The Figure 15 also shows a cross-section of the proposed thin-film battery. The battery is fabricated onto an insulating substrate, by successive film depositions of the metal current collectors, cathode, electrolyte and anode. The depositions of these layers were made by sputtering (Direct Current, DC and Radio-frequency, RF). A protective coating of silicon nitride (Si_3N_4) is required to prevent the reaction of lithium when the battery is exposed to the air (Dudney *et al*, 1999). A silicon substrate will be used for integration with microelectronics, while at same time providing good thermal contact with heat source and sink.
Lithium cobaltate ($LiCoO_2$) was the compound chosen as cathode, due to its excellent electrochemical cycling stability, which is a result of the structural stability of the material, in which the layered cation ordering is extremely well preserved even after a repeated process of insertion and extraction of lithium ions (Park *et al*, 2008).
For the electrolyte deposition, it was used the lithium phosphorus oxynitride (Li_3PO_4N or Lipon). The material used for the electrolyte deposition is the lithium phosphate, whose chemical formula is Li_3PO_4. After the sputtering deposition with a N_2/Ar plasma a Lipon is obtained. This electrolyte has an acceptable ionic conductivity, which is about 2×10^{-6} Scm^{-1}. In addiction, Lipon films presents an electronic resistivity greater than 10^{14} Ωcm, which helps to minimise the short circuit self-discharge and increasing the battery's life (Dudney, 2005).
Tin dioxide (SnO_2) was chosen for the anode material due to their high-lithium storage capacity and low potential of lithium ion intercalation. A tin dioxide anode can give a maximum theoretical 781 $mAhg^{-1}$ charge-storage capacity (Wang *et al*, 2005). Also, the average resistivity of tin dioxide films are in the

range 10-17 mΩ.cm for films with thickness less than 100 nm. However, for values of the thickness greater than 100 nm, the values fall in the range 5-9 mΩcm.

Target applications for energy scavenging systems with thin-films batteries and thermoelectric converters are in wireless nodes of wireless sensors networks. Energy harvested wireless sensors must be powered in a peak basis because a temperature gradient could not always be present, thus the energy must be stored in a rechargeable microbattery integrated in the system (Alahmad *et al*, 2008). Ultra-low power electronics performs DC-DC rectification with a variable conversion factor. The Figure 16 shows a simple step-up converter. The step-up conversion is made with the help of the capacitor C_{up} and the inductor L_{up}. The current at the output of the thermoelectric microdevice charges this capacitor, then the switch SW is systematically closed and open, with a fast frequency. However, it remains closed during a very short time in order to reduce the losses. In order to meet this requirement, the command signal must have a very low duty-cycle to avoid the over-discharge of the capacitor C_{up}. When SW opens, the stored energy in the inductor L_{up} forces the capacitor C_{up} to discharge through the diode D, e.g., a DC rectification is present. Then, the current charges the high-charge-capacity capacitor, C_{store}, which further connects to a DC regulator.

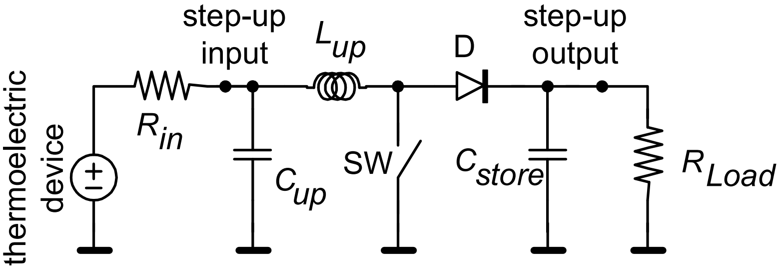

Figure 16: Schematic of a simple step-up circuit.

A more interesting solution was implemented, using components off-the-shelf. The Figure 17(a) shows the electronic schematic of a circuit prototype to do DC-DC step-up conversion, which uses the S-882Z and S-8353 circuits from the Seiko Manufacturer (Mateu *et al*, 2007). The photographs in the Figure 17(b) are the bottom and top planes of the final prototype mounted with the several components. This circuit was tested to evaluate its electrical behaviour. The Table II lists the whole set of tests (for several input voltages and currents) and it can be observed (except for the situation where V_{out}=4.50 V) that in spite of the maximum 3.70 V of a lithium battery not be present, the output voltage approaches such a value. The efficiency of the circuit is always above 85%, thus its loss of power inside is acceptable.

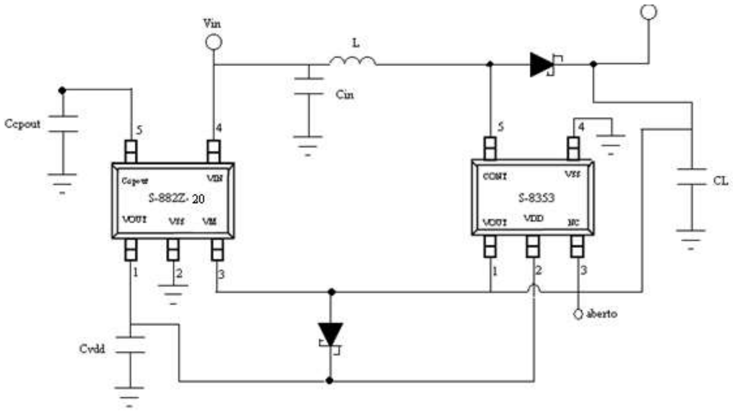

(a)

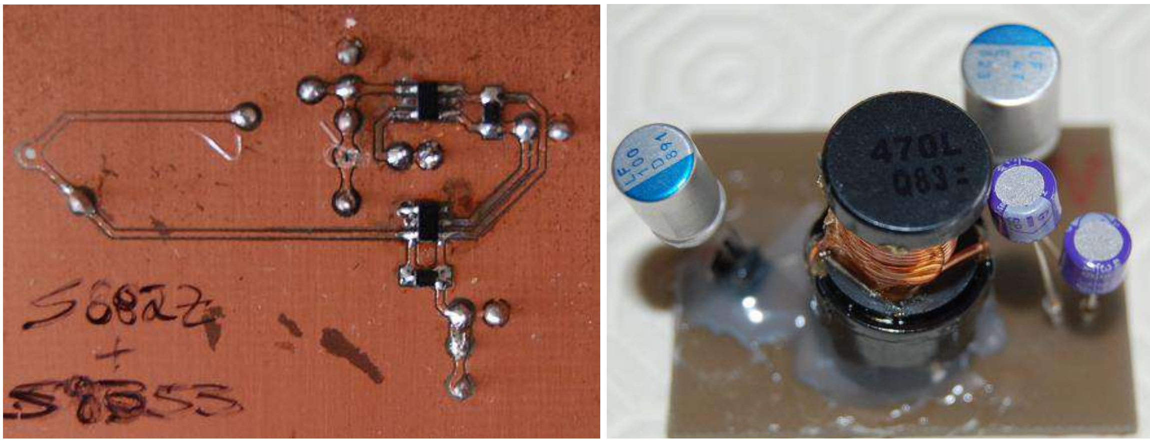

(b)

Figure 17: A circuit prototype of a DC-DC step-up conversion, using the S-882Z and the S-8353 circuits from Seiko: (a) schematic and (b) the bottom and top planes of the fabricated prototype.

Table II: The set of tests done to the DC-DC converter circuit.

V_{in} [V]	I_{in} [ma]	V_{out} [V]	I_{out} [ma]	P_{in} [mW]	P_{out} [mW]	η [%]
0.31	40.11	3.20	3.32	12.43	10.62	0.85
0.39	45.30	3.40	5.05	17.57	17.17	0.98
0.45	50.50	3.60	5.91	22.70	20.68	0.91
0.50	70.10	4.50	7.55	35.05	33.97	0.97

Thin-film solid-state batteries show a very high-life cycle and are intrinsically safe. This is of special concern in the design of thermoelectric energy scavenging microsystems, mainly when the thought applications are in the biomedical field or for long cycle operations without requiring human activity.

CONCLUSIONS AND FUTURE DEVELOPMENTS

In today's best commercial thermoelectric modules (specifically for the compounds made of antimony and tellurium presented in this chapter) the figure-of-merit, *ZT*, is about one, despite many approaches to find compounds with higher performance. In conventional 3D crystalline systems it is difficult to control each of the following are interrelated factors to improve *ZT* .This means that an increase of the Seebeck voltage per unit of temperature, usually results in a decrease of the electrical conductivity. Moreover, a decrease of the electrical conductivity leads to a decrease of the electronic contribution to the thermal conductivity, following the Wiedemann-Franz law. However, if the dimensionality of the material is decreased, the new variable of length scale becomes available for the control of materials properties, due to differences in the density of electronic states. Recent work with antimony/bismuth/tellurium superlattices demonstrated an enhancement in the *ZT* to about 2.4 (Venkatasubramanian *et al*, 2001). Thermoelectric micro devices with high figures of merit, based on superlattices are the key to generate power from low temperature gradients, and to produce high temperature gradients with a low-power supply. This will opens doors to automotive and domestic applications, where high heat flows are present as well as the operation at higher temperatures.

REFERENCES

Alahmad, M., et al. (2008). Evaluation and analysis of a new solid-state rechargeable microscale lithium battery. IEEE Transactions on Industrial Electronics, 55, 3391-3401.

Armand, M., and Tarascon, M. (2008). Building better batteries. *Nature, 451*, 652-657.

Birkholz, U., *et al.* (1987). Fast semiconductor thermoelectric devices. *Journal Sensors and Actuators A, 12*, 179-184.

Carmo, J. P., *et al.* (2009). *Integrated thin-film rechargeable battery in a thermoelectric scavenging microsystem*. in Proc. Powereng 2009, Lisbon, Portugal, 359-363.

da Silva, L., and Kaviany, M. (2002). *Miniaturized thermoelectric cooler*. in Proc. IMECE 2002 - 2002 ASME International Mechanical Engineering Congress & Exposition. New Orleans, Louisiana, USA. Paper No. 2-8-1-6.

da Silva, L., and Kaviany, M. (2004). Micro-thermoelectric cooler: interfacial effects on thermal and electrical transport. *Internacional Journal Heat Mass Transfer, 47*, 2417–2435.

da Silva, L., *et al.* (2005). Thermoelectric performance of films in the bismuth-tellurium and antimony-tellurium systems. Journal of Applied Physics, 97. 114903.

Dudney, N. J. (2005). Solid-state thin-films rechargeable batteries. *Materials Science & Engineering B, 116*, 245-249.

Dudney, N. J., and Neudecker, B. J. (1999). Solid state thin-films lithium battery systems. *Solid State & Materials Science, 4*, 479-482.

Dyck, J. S., *et al.* (2002). Heat transport in $Sb_{2-x}V_xTe_3$ single crystals. *Physical Review B*, *66*, 125206.

Goncalves, L. M., *et al.* (2006a). Optimization of thermoelectric thin-films deposited by coevaporation on plastic substrates. in Proc. ECT'06, Cardiff, UK, 2006.

Goncalves, L. M., *et al.* (2006b). Flexible thin-film planar Peltier microcooler. in Proc. of ICT'06, Vienna, Austria, 2006.

Goncalves, L. M., *et al.* (2008a). Thermoelectric Micro Converters for Cooling and Energy Scavenging Systems. *Journal Micromechanics and Microengineering, 18*.

Goncalves, L. M., *et al.* (2008b). On-chip array of thermoelectric Peltier microcoolers, *Journal Sensors and Actuators A, 145-146*, 75-80.

Goncalves, L. M., *et al.* (2011). Thermal co-evaporation of Sb2Te3 thin-films optimized for thermoelectric applications, *Thin Solid Films, Accepted for publication on 2011*, 1-6.

JCPDS. (1983). Joint Committee on Powder Diffraction Standards (JCPDS), Powder Diffraction File, Pennsylvania.

L. Mateu, *et al.* (2007). *Human body energy harvesting thermogenerator for sensing applications.* in Proc. 2007 International Conference na Sensor Technologies and Applications, Valencia, Spain.

Park, M., *et al.* (2008). Performance evaluation of printed LiCoO2 cathodes with PVDF-HFP gel electrolyte for lithium ion microbatteries. *Electrochimica Acta, 53*, 5523-5527.

Peltier, J. C. (1834). Nouvelles experiences sur la caloricité des courans électriques. *Annales de Chimie et the Physique, LVI 56*, 371-386

Scherrer, H., and Scherrer, S.. (1995). Bismuth Telluride, Antimony Telluride and Their Solid Solution. Handbook of thermoelectrics, edited by D.M. Rowe, CRC Press, 211-237.

Seebeck, T. I. (1822). Magnetische polarisation der metalle und erze durch temperatur-differenz. *Abhandlungen der Deutschen Akademie der Wissenschaften zu Berlin*, 265-373.

Venkatasubramanian, R., *et al.* (2001). Thin-film thermoelectric devices with high room-temperature figures of merit. *Nature, 413*.

Völklein, F., and Stärz, T. (1997). *Thermal Conductivity of Thin Films - Experimental Methods and Theoretical Interpretation.* in Proc. 16th International conference on Thermoelectrics, 711-718.

Wang, Z., *et al.* (2005). Coating of multi-walled carbon nanotube with SnO2 films of controlled thickness and its application for Li-ion battery. *Journal of Power Sources*.

Zou, H., *et al.* (2002). Peltier effect in a co-evaporated Sb_2Te_3(P)-Bi_2Te_3(N) thin film thermocouple. Thin Solid Films, 408, 270-274.